Influence of the nature of the anchoring group on the interfacial energy level alignment in dye-sensitized solar cells: A theoretical perspective

Imane Arbouch [1,2] Yasser Karzazi [1] and Jérôme Cornil [2]

[1] *Laboratoire de Chimie Analytique Appliquée, Matériaux et Environnement (LC2AME), Faculté des Sciences, Université Mohammed Premier, B.P. Box 4808, 60046 Oujda, Maroc*

[2] *Laboratory for Chemistry of Novel Materials, University of Mons, Place du Parc 20, B-7000 Mons, Belgium*

(Received 1 July 2020; accepted 2 October 2020; published 6 November 2020)

We investigate at the theoretical (time-dependent) density functional theory level the influence of the nature of the anchoring group on the electronic and optical properties of oligothiophene dyes when adsorbed on TiO_2 surface. The computed electronic structures point to a strong orbital hybridization between the dye and the substrate in the presence of the carboxylic acid and thiocarboxylic acid group, leading to a pronounced pinning effect of the lowest unoccupied molecular orbital (LUMO) level and faster electron injection. In contrast, phosphonic acid and catechol promote a weak electronic coupling between the two components and hence slower injection times. The simulated absorption spectra demonstrate that carboxylic and thiocarboxylic anchoring groups can induce a large redshift of the lowest optical transition of the dye upon adsorption due to a strong stabilization of the LUMO level triggered by the pinning effect while a small redshift prevails for phosphonic and catechol dyes. When pinning is active, the chain-size evolution of the lowest optical transition is also less sensitive to the conjugation length compared to the free dyes.

DOI: 10.1103/PhysRevMaterials.4.115401

I. INTRODUCTION

Since their invention by Grätzel and O'Regan in 1991 [1], dye-sensitized solar cells (DSSCs) have attracted a growing scientific and economic interest as one of the potential low-cost photovoltaic devices [2,3]. The fabrication of DSSCs is simple and uses abundant and low-cost materials with an estimated production cost between \$1 and \$0.5 per peak watt (W_p), which is largely lower than $\$7/W_p$ estimated for conventional silicon solar cells. A dye sensitized solar cell corresponds to a photoelectric device that mimics photosynthesis in order to produce electrical energy from sunlight. In a typical *n*-type DSSC, the dye sensitizer anchored on the surface of a wide band-gap semiconductor (typically TiO_2 or, less commonly, ZnO) absorbs the sunlight and generates an excited state from which the electron is transferred to the conduction band of the semiconductor. The oxidized dye is neutralized by a redox mediator, which is in turn regenerated at the counter electrode. The reported energy conversion efficiencies of DSSCs have reached 12% for those sensitized by ruthenium dyes [4] while substituting the dye sensitizers by organic-inorganic perovskite materials has increased the DSSCs energy conversion efficiency higher than 25% [5]. Importantly, the perspective of cheap production as well as the perpetual improvements in device stability drive the growth of dye-sensitized solar cells further in a dynamic way and make them a real alternative to silicon-based solar cells.

Dyes sensitizers are at the heart of the operation of DSSCs. Thus, a great deal of attention has been paid in selecting and developing ideal candidates. On the one hand, metal complexes have been extensively investigated and applied as sensitizers in DSSCs owing to their broad absorption spectrum, suitable excited-state energies, long excited-state lifetime, and good chemical stability. To date, ruthenium [Ru (II)] complexes have yielded the best photovoltaic performance among the metal complexes [6–11]. The most attractive ruthenium complexes are the $RuL_2(NCS)_2$ complex (N3 dye) [12–14] and $RuL'(NCS)_3$ complex (Black dye) [15–17] that have reached efficiencies that exceed 11%. On the other hand, organic dyes are a good alternative to the Ru complexes dyes mainly due to their lower production cost and their large absorption coefficients related to the intramolecular π-π^* transitions. Generally, a donor-π-bridge-acceptor (D-π-A) molecular structure is used, with the electron-rich donor group (D) linked through a conjugated bridge (π) to the electron-poor acceptor group (A). To date, hundreds of organic dyes, including coumarin dyes [18,19], indoline dyes [20,21], tetrahydroquinoline dyes [22,23], perylene dyes [24,25], and oligothiophene dyes [26,27], have been tested as sensitizers for DSSCs.

The performance of DSSCs is strongly dictated by the efficiency of various electron processes (see green lines in Fig. 1), namely electron transfer from the dye to the semiconductor and electron transport through the semiconductor and dye regeneration. Several loss mechanisms (see red lines in Fig. 1) such as electron recombination with the dye or with the redox moiety (back transfer) and dye deexcitation limit the overall efficiency of DSSCs and have thus to be minimized.

The electron transfer from the dye to the semiconductor is a determining process in the operation of DSSCs. Several experimental and theoretical studies have demonstrated that two types of injection mechanisms may be operative in

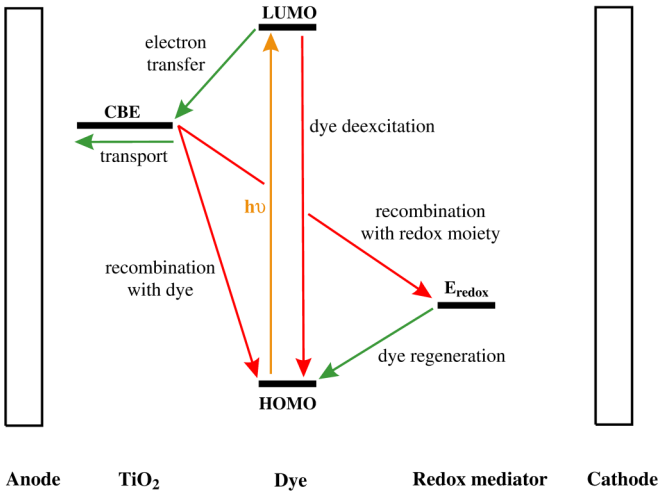

FIG. 1. Schematic representation of the different kinetic processes competing in a dye-sensitized solar cell.

DSSCs [28–30]. The first mechanism (type I) is an indirect injection occurring in a two-step process, with first a photoexcitation of the dye (orange line in Fig. 1) followed by electron transfer from the lowest unoccupied molecular orbital (LUMO) of the dye to the semiconductor conduction band, in a simple one-electron picture. The second mechanism (type II) is a direct photoexcitation from the dye ground state to the conduction band of the semiconductor without any implication of the intramolecular dye excited states [28,31,32]. The latter mechanism is characterized by the appearance of new low-energy bands in the absorption spectra. In fact, most dyes operating via the type-II mechanism can also inject electrons to TiO_2 through a type-I pathway so that the photovoltaic current generated from the so-called type-II DSSCs is inevitably generated by both mechanisms (type I and type II) [33–36]. The type-II mechanism should lead to an effective electron injection because it takes place directly from the dye ground state to the semiconductor conduction band. However, the back-electron transfer (recombination with dye) from the lowest excited charge-transfer state is also favored since the electronic levels that are implicated in both the excitation and recombination processes are similar [37]. As a result, the efficiency of the type-II mechanism is highly limited compared to the type-I mechanism. The rates of electron transfer processes have been experimentally measured for several dyes by using accurate techniques such as resonant photoemission [38], Raman spectroscopy [39], fluorescence up-conversion spectroscopy [40], and two photon photoemission spectroscopy [41,42]. These results reveal that the electron injection from the dye to the semiconductor conduction band typically occurs in a few-femtosecond times scale while the recombination process takes place in a hundred picoseconds to nanoseconds.

The dye sensitizers in DSSCs contain one or more chemical groups that may act as anchoring units allowing their adsorption onto the semiconductor. The anchoring group may also affect the injection rate by playing the role of an electron transfer mediator between the sensitizer and the semiconductor [43,44]. Carboxylic acid and cyanoacrylic acid groups are the most exploited anchoring group [45]. However, with the recent advances in DSSCs, many other anchoring groups have emerged, which has considerably extended the choice of materials and contributed in the understanding of the complex interface between the dye and the semiconductor. In this respect, our group has theoretically explored the adsorption of oligothiophene dyes of increasing chain length through a carboxylic acid anchoring group on a titanium dioxide anatase (101) model surface [46]. These calculations evidenced that the adsorption leads to a noticeable pinning effect for the LUMO of the dye, i.e., the energy level alignment of the LUMO with reference to the titania conduction-band edge (CBE) is slightly sensitive to the conjugation length due to a strong interfacial orbital hybridization, conversely to the situation reigning for the free oligomers. A considerable implication of this pinning effect revealed by time-dependent density functional theory (TD-DFT) calculations is that the absorption spectrum of the dye can be radically different when going from solution to the adsorbed system, thus possibly ruining all efforts made in molecular design to match the solar emission spectrum. Interestingly, the pinning effect is strongly attenuated when anchoring the molecules via a catechol group [47]. Noteworthy, the interfacial energy level alignment at the dye-titania interface is extremely relevant for the physics of DSSCs devices since it affects the injection times (and therefore the short-circuit current J_{SC}) and thus the global efficiency of DSSCs [48,49].

This has motivated the present paper in which we have extended our earlier theoretical study to compare the influence of four widely used anchoring groups (namely carboxylic acid, thiocarboxylic acid, phosphonic acid, and catechol) on the change in the electronic and optical properties of oligothiophene dyes adsorbed on a titania model cluster. In contrast to our previous studies, the larger number of data accumulated here allows us to gain a much deeper insight into the key parameters controlling the interfacial energy level alignment. This paper is organized as follows. The theoretical models and the computational methodology are described in Sec. II. In Sec. III, we present and discuss the results of our calculations. The interactions at the dye-semiconductor interface were examined by using the Newns-Anderson model. The energy level alignment of the dye LUMO with respect to the TiO_2 conduction-band edge and its lifetime broadening were derived from the calculated electronic structures and utilized to evaluate the pinning effect strength and estimate the electron injection times into the conduction band of TiO_2. Finally, the optical response of the free versus adsorbed dyes is examined.

II. MODELS AND COMPUTATIONAL METHODOLOGY

A. Titanium dioxide and free protonated oligothiophene dyes

A primordial advance in modeling anatase nanocrystals by using suitable cluster models of the TiO_2 surface has been achieved by Lundqvist *et al.* [50], who studied the structural and electronic properties of $(TiO_2)_n$ clusters and nanoparticles with size of approximately 2 nm by means of DFT calculations. Large cluster models have been constructed by following two steps: (1) the anatase crystal structure unit cell, that contains 12 atoms [51] has been expanded in all three

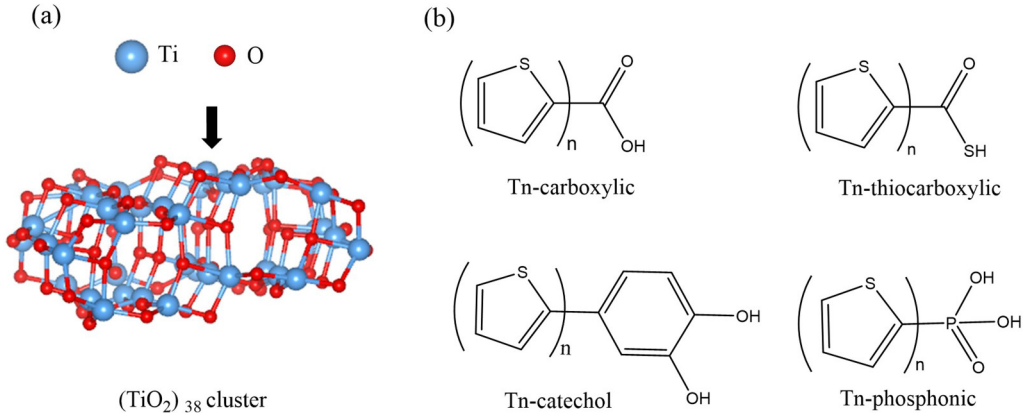

FIG. 2. Molecular structures of (a) $(TiO_2)_{38}$ cluster and (b) oligothiophene dyes.

dimensions, and (2) the Ti and O atoms have been removed such as the obtained cluster is stoichiometric, charged neutral, and with a coordination of every Ti and O atom as high as possible [52]. In this work, we modeled the anatase titanium dioxide (101) surface as described in Refs. [53,54]. The cluster model $(TiO_2)_{38}$ [55] is stoichiometric, neutral, nonpolar, and constructed from two TiO_2 layers with alternating rows of five- and sixfold coordinated titanium sites [see Fig. 2(a)]. The choice of $(TiO_2)_{38}$ cluster model has been driven by its ability to successfully reproduce the electronic properties of TiO_2 nanoparticles [53].

For organic dyes, we have selected a series of oligothiophene derivatives with an increasing number (n) of monomer units (n running from 1 to 5) featuring different anchoring groups, namely carboxylic acid, catechol, thiocarboxylic acid, and phosphonic acid [see Fig. 2(b)]. These systems allow the investigation of the influence of the anchoring group nature as well as the effect of the chain size on the electronic and optical characteristics of oligothiophene dyes upon their adsorption on $(TiO_2)_{38}$ cluster.

B. Binding modes of the anchoring groups

The strength of the dye adsorption mediated by the anchoring group is one of the determining factors that affects the long-term stability of DSSCs [44]. The adsorption geometry of dyes on TiO_2 has been extensively investigated theoretically and experimentally [3,56–59]. For our selected dyes, the anchoring group may adopt several chemisorption modes. As displayed in Fig. S1 of the Supplemental Material [63], carboxylic acid, thiocarboxylic acid, and catechol adsorb on anatase (101) with three possible binding modes: monodentate, chelating bidentate, or bridging bidentate, while phosphonic acid may also adopt a tridentate adsorption on anatase (101) with three oxygens bonded each to a different titanium atom [45,56,60]. Experimentally, the adsorption modes can be assessed by specific characterization tools such as Fourier transform infrared spectroscopy (FTIR) in transmission geometry, attenuated total reflectance FTIR (ATR-FTIR) [58], photoelectron spectroscopy (PES) [61], and photoemission and near-edge x-ray-absorption fine structure (NEXAFS) [62]. These experiments can be further complemented by computational chemistry to assess the relative stability of the different binding motifs. In this work, we have investigated by means of density functional theory (DFT) calculations with the B3LYP functional and a 6-311G* basis set the most stable adsorption mode for our anchoring groups on the titania anatase (101) surface through the evaluation of adsorption energies. It is worth mentioning that the tridentate geometry of phosphonic acid suffers from a bad geometrical match since the distance to a third coordinatively unsaturated Ti is too large so that no stable structure can be obtained [59]. Thus, this configuration has been excluded from the calculations.

The adsorption energy is calculated by computing the difference in energy between the total energy of the adsorbed system (TiO_2 + adsorbate) and the bare TiO_2 cluster plus the free protonated adsorbate in the gas phase as expressed in Eq. (1):

$$E_{\text{ads}} = E_{[\text{TiO}_2,\ \text{adsorbate}]} - E_{[\text{TiO}_2]} - E_{[\text{adsorbate}]}. \qquad (1)$$

The results detailed in Sec. I of the Supplemental Material [63] reveal that the bridging bidentate geometry has the largest adsorption energy for the four anchoring groups, thus motivating our exclusive focus on this adsorption mode in the following.

III. COMPUTATIONAL DETAILS

In order to simulate the electronic and optical properties of our free and adsorbed systems, three sets of calculations have been performed as follows:

(1) The ground-state geometry of the free dye molecules (protonated dye molecules), the bare TiO_2 cluster, and the adsorbed systems (TiO_2 cluster + dye molecules) have been optimized by using the Perdew-Burke-Ernzerhof (PBE) functional with the generalized gradient approximation (GGA) [64] and a double-zeta basis set, with the Amsterdam density functional (ADF) package [65]. Note that the B3LYP functional was used in our previous study only for the geometry optimization of the free dye [47], thus explaining the variations in the numbers reported for adhesion energies and level energies of the free dyes between the studies. The results presented here are more meaningful in view of the coherence in the geometry optimization procedure.

(2) For the sake of coherence with our previous studies [46,47], the electronic structure of all systems has been next computed by single-point calculations on these optimized geometries by employing the hybrid B3LYP functional and a standard 6-311G* basis set with Gaussian 09 [66]. It is worth emphasizing that the solvent effects were not included in our calculations since common solvents such as acetonitrile, water, methanol, and chloroform were found to provide very similar results in our previous study [46], which motivates us to simply perform calculations in the gas phase. Moreover, no dispersion corrections were accounted for since we are dealing here with chemisorbed systems, with the molecules standing perpendicular to the substrate.

(3) Taking advantage of the cluster approach, The UV absorption spectra of the full systems have been simulated using here the TD-DFT formulation with the same hybrid B3LYP functional and 6-311G* basis set.

A. Dye-titania electronic interactions

To analyze the dye-semiconductor interactions, we use the Newns-Anderson approach for adsorbates on surfaces [67] as formulated by Persson *et al.* [68]. This model evaluates the effect of the adsorption process on the dye electronic levels (basically only the dye LUMO level is examined) in terms of an energetic shift with respect to the free dye and a lifetime broadening. This lifetime broadening is described by a Lorentzian distribution characterizing the decay of the dye LUMO coupled to the conduction-band states of the TiO_2. To measure these two quantities, an evaluation of the projected density of states (PDOS) of the LUMO level is required. Typically, a molecular orbital ψ_i is defined by the expression

$$\psi_i = \sum_j^n c_{ij}^A \, \chi_j^A, \tag{2}$$

where χ_j^A are the atomic orbitals centered on a given atom A and c_{ij}^A are the expansion coefficients.

The adsorbate fraction p_i^{ads} of a MO, i, with an orbital energy ϵ_i is defined as the sum of the squares of the atomic orbital coefficients that belong to the adsorbate (ads) atoms [68].

$$p_i^{\text{ads}} = \sum_j^{A \in \text{ads}} \left(c_{ij}^A\right)^2 \Big/ \sum_j^n \left(c_{ij}^A\right)^2. \tag{3}$$

An energy interval is then selected within which the virtual molecular orbitals feature the signature of the shape of the LUMO in the free dye. This energy interval was selected so that the sum of the adsorbate fraction PDOS within this interval is close to 1 within typically 2%: $\sum p_i^{\text{ads}} \approx 1$.

The center of this distribution is the energy of the dye LUMO E_{LUMO} (ads), that can be calculated as a weighted average:

$$E_{\text{LUMO}}(\text{ads}) = \sum_i p_i^{\text{ads}} \epsilon_i. \tag{4}$$

The induced energy shift is calculated as

$$\Delta E = E_{\text{LUMO}}(\text{ads}) - E_{\text{LUMO}}(\text{free}), \tag{5}$$

TABLE I. Adsorption energies (kcal/mol) for Tn dyes adsorbed on the TiO_2 cluster. Values for carboxylic acid, thiocarboxylic acid, catechol, and phosphonic acid alone are also presented for sake of comparison.

Dyes	E_{ads}	Dyes	E_{ads}	Dyes	E_{ads}	Dyes	E_{ads}
Carb	−41	thio	−35	cat	−54	phos	−53
T1-carb	−40	T1-thio	−34	T1-cat	−54	T1-phos	−54
T2-carb	−42	T2-thio	−34	T2-cat	−54	T2-phos	−53
T3-carb	−42	T3-thio	−34	T3-cat	−54	T3-phos	−54
T4-carb	−41	T4-thio	−30	T4-cat	−53	T4-phos	−52
T5-carb	−41	T5-thio	−31	T5-cat	−54	T5-phos	−53

where E_{LUMO} (free) can be obtained from an electronic calculation on the free dye.

The width of the LUMO (ads) broadening can be quantified as a mean deviation of a distribution centered at the LUMO (ads) level:

$$\hbar\Gamma = \sum_i p_i^{\text{ads}} |\epsilon_i - E_{\text{LUMO}}(\text{ads})|. \tag{6}$$

A Lorentzian distribution ρ_{LUMO} is then constructed from

$$\rho_{\text{LUMO}}(E) = \frac{1}{(E - E_{\text{LUMO(ads)}})^2 + \left(\frac{\hbar\Gamma}{2}\right)^2}. \tag{7}$$

The electron transfer time can be directly estimated by the LUMO lifetime broadening through the time-energy uncertainty relation $\tau(fs) = \hbar/\hbar\Gamma$ [67], which in convenient numerical units becomes

$$\tau(fs) = 658/\hbar\Gamma \text{ (meV)}. \tag{8}$$

IV. RESULTS AND DISCUSSION

A. Adsorption energies

As detailed in the previous section, the adsorption energies of the oligothiophene dyes on the titania cluster can be calculated by using Eq. (1) (see Table I). The computed adsorption energy for carboxylic acid, thiocarboxylic acid, catechol, and phosphonic acid alone are also reported in order to assess their contribution to the adsorption energy. The binding strengths of the oligothiophene dyes on the anatase (101) surface depend strongly on the nature of the anchoring group (varying by as much as 14 kcal/mol) and are ordered as follows: Tn-phosphonic acid, Tn-catechol > Tn-carboxylic acid > Tn-thiocarboxylic acid. In agreement with our results, experimental investigations have evidenced that phosphonic acid has a tendency to bind the dyes more strongly to the surface than carboxylic acid, thus offering better long-term stability [69]. Our results are also in line with previous theoretical studies. Indeed, the adsorption energies of phosphonic acid and carboxylic acid on the anatase (101) surface have been investigated in another study using hybrid DFT calculations by using B3LYP functional and a split-valence basis set, reaching the conclusion that the adsorption of phosphonic acid is significantly stronger by 18 kcal/mol compared to carboxylic acid [70]. Ambrosia *et al.* [44] have theoretically compared

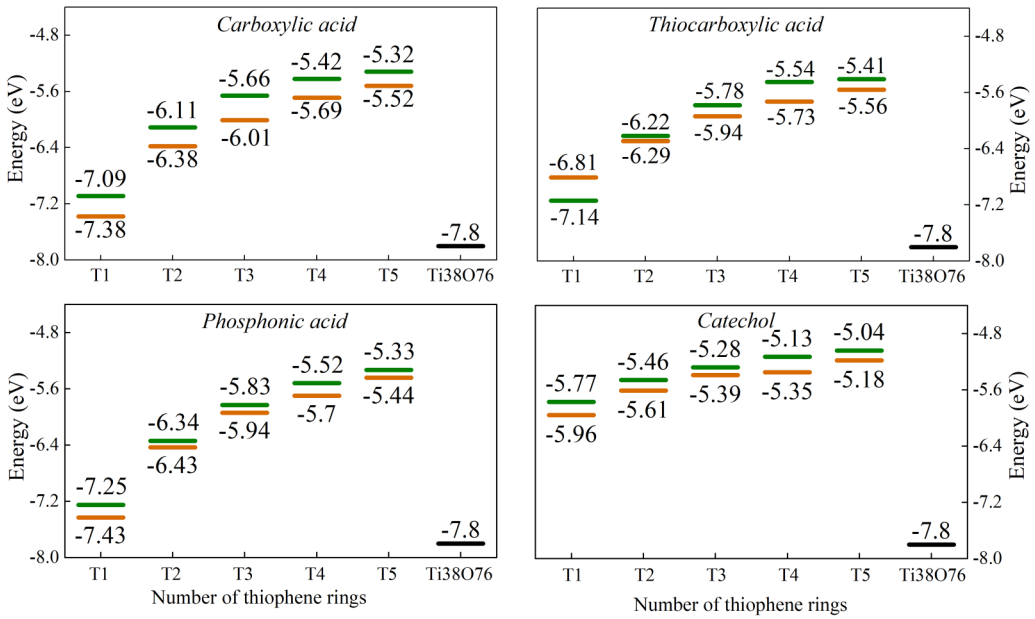

FIG. 3. HOMO energy levels for the free (green line) and adsorbed (orange line) Tn dyes. The value of the valence-band edge of bare TiO_2 is also indicated (black line).

the adsorption of perylene on the anatase (101) surface via different anchoring groups using a periodic boundary description of TiO_2 slabs based on the PBE functional; they found that phosphonic acid exhibits the strongest adsorption energy among all the investigated anchoring groups. Another DFT study has investigated the adsorption of catechol on anatase (101) surface and found an adsorption energy of 52 kcal/mol [71], in good agreement with our calculated adsorption energy of 54 kcal/mol. That carboxylic acid and thiocarboxylic acid exhibit the smallest adsorption energies, with carboxylic acid giving a slightly larger adsorption energy than the thiocarboxylic acid, is also in agreement with the calculations of Ambrosia *et al.* [44] predicting that thiocarboxylic acid exhibits an adsorption energy almost similar to that of the carboxylic acid for adsorbed perylene dyes on titania.

More importantly, the calculated adsorption energies of the oligothiophene dyes are similar to the adsorption energies of the sole anchoring group. For example, the calculated adsorption energy of 34 kcal/mol (53 kcal/mol) for the T2-thiocarboxylic (T2-phosphonic) dye is similar to the adsorption energy of the anchoring group alone of 35 kcal/mol (53 kcal/mol) for thiocarboxylic acid (phosphonic acid). These results clearly demonstrate that the binding of larger dye molecules on the substrate surface are well evaluated from the binding strength of the sole anchoring group on that surface.

B. Energy level alignment

The energy level alignment at dye-titania interfaces is a key parameter ruling the rates of the interfacial electron transfer processes in DSSCs. The driving force for electron injection is determined by the energy gap between the dye LUMO and the conduction-band edge (CBE) of titania. Any change in the relative energetic position of the molecular-orbital levels of the dyes upon adsorption on TiO_2 surface illustrates the hybridization strength between the molecular orbitals and the conduction-band states of the semiconductor. More importantly, the optical response is likely to be affected by changes in the HOMO-LUMO gap of the dye molecule upon adsorption. As a first step, we have investigated the impact of adsorption on the energetic position of the HOMO level. The energetic position of the HOMO of the oligothiophene dyes before and after adsorption on titania cluster as a function of the number of thiophene rings (n) is displayed in Fig. 3.

Despite the energy stabilization of the HOMO levels of Tn dyes upon adsorption on titania, the electronic interaction with the substrate is considered to be weak since the HOMO levels of free dyes stand in the band gap of the TiO_2 semiconductor (-7.8 eV for the top of the VB and -3.6 eV for the bottom of the CB). In fact, the shape of the HOMO levels for the T2 adsorbed dyes displayed in Fig. 4 plainly shows that the electronic density of the HOMOs is mostly localized on the dye part with no noticeable mixing between the dye and the titania surface.

This behavior is in accordance with the Newns-Anderson model reporting that when a discrete level of the molecule (here the HOMO) lies energetically in the band-gap region of the substrate (here TiO_2), that molecular orbital weakly hybridizes with the band states.

The electron transfer time from the dye to the TiO_2 surface is largely governed by the electronic coupling strength between the injecting orbital (the dye LUMO) and the conduction-band states of TiO_2 cluster. In the Newns-Anderson model, and since the LUMO levels of the free dyes stand within the conduction band of the semiconductor, the strength of this interaction can be evaluated by the energetic shift of the dye LUMO relative to the free dye [ΔE given in Eq. (5)] and its lifetime broadening [($\hbar\Gamma$ given in Eq. (6)].

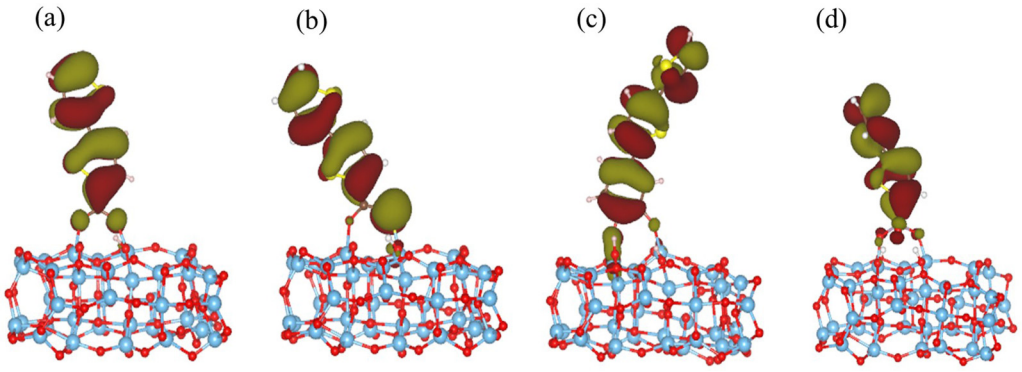

FIG. 4. Shape of the HOMO orbitals of the adsorbed (a) T2-carboxylic, (b) T2-thiocarboxylic, (c) T2-catechol, and (d) T2-phosphonic.

The computed energetic positions of the LUMO for both free and adsorbed Tn dyes are displayed in Fig. 5. The conduction-band edge of the titania cluster in the adsorbed systems and that of the bare titania cluster are also shown for the sake of reference.

The energy alignment of the dye LUMO with the conduction-band edge of titania displayed in Fig. 5 reveals that the dye LUMO is systematically in resonance with the conduction band and still at higher energies with respect to the conduction-band edge of the titania cluster, as required for an effective electron injection. Strikingly, Fig. 5 shows that a slight lowering of the LUMO level is noticed for phosphonic dyes (less than 0.26 eV) and catechol dyes (less than 0.15 eV) when going from the free to adsorbed system while a larger lowering is observed for carboxylic (more than 0.34 eV) and thiocarboxylic dyes (more than 0.29 eV). In order to understand this discrepancy in behaviors, we have presented in Fig. 6 the shape of the electronic level in the T2 adsorbed system featuring the largest signature of the dye LUMO. Figure 6 reveals that the LUMOs of catechol and phosphonic dyes display only a weak electronic density on the anchoring group, while the LUMOs of the adsorbed carboxylic and thiocarboxylic dyes are expanded over the anchoring group, which points to a stronger hybridization in the latter case and thus rationalizes the larger energy shifts.

In addition to the larger energy shift of the dye LUMO upon adsorption found for carboxylic and thiocarboxylic dyes, the strong electronic coupling between the dye and titania is also reflected by the length dependence of the energy of the LUMO level in the adsorbed systems relatively to the corresponding free dyes. Hereafter, we characterize this evolution by an S ratio defined as

$$S = \frac{\Delta\left(E^{T1}_{\mathrm{LUMO}} - E^{T5}_{\mathrm{LUMO}}\right)_{\mathrm{adsorbed}}}{\Delta\left(E^{T1}_{\mathrm{LUMO}} - E^{T5}_{\mathrm{LUMO}}\right)_{\mathrm{free}}}, \tag{9}$$

where E^{T1}_{LUMO} is the LUMO energy of the T1 dye while E^{T5}_{LUMO} is the LUMO energy of the T5 dye. If the S ratio is close to

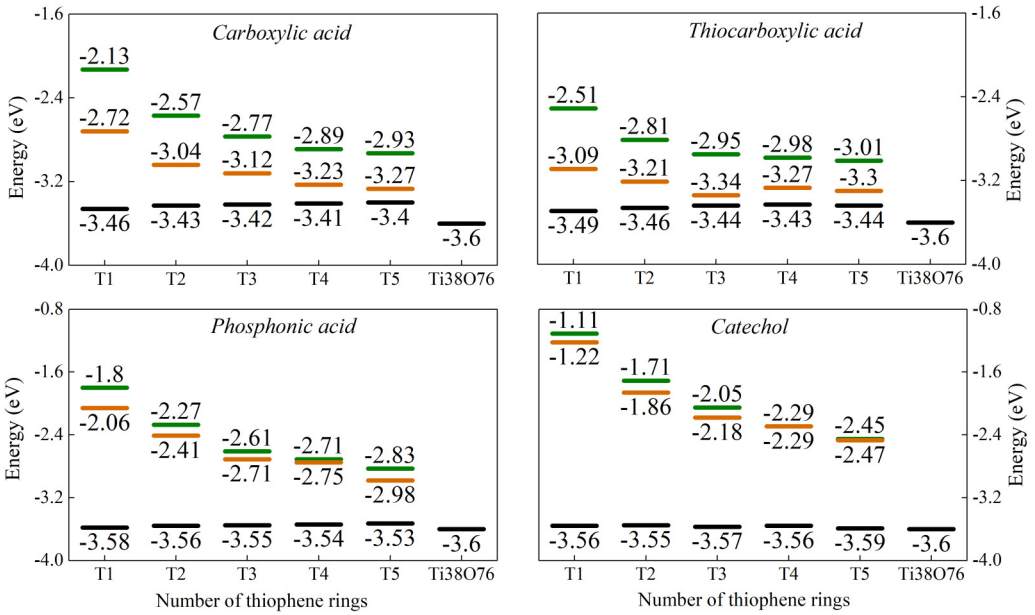

FIG. 5. LUMO energy levels for the free (green line) and adsorbed (orange line) Tn dyes. The energy of the conduction-band edge in all cases is also reported (black line) for the sake of reference.

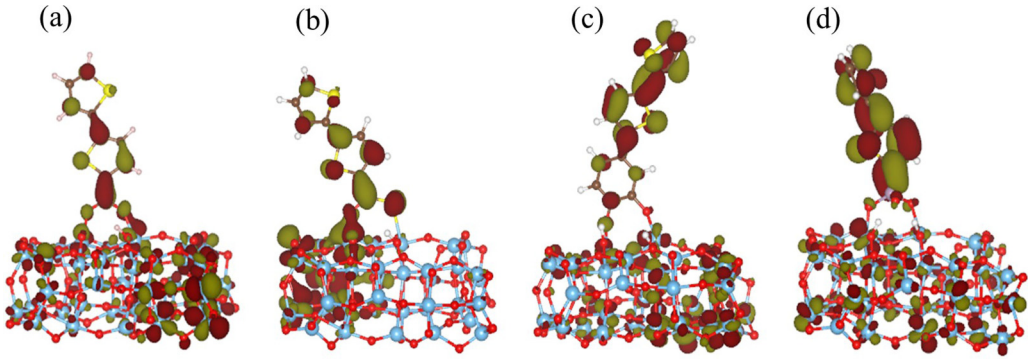

FIG. 6. Shape of the selected LUMO orbitals: (a) The LUMO+11 of T2-carboxylic dye located at −3.11 eV (with 17% of electron density localized on the dye part), (b) the LUMO+6 of T2-thiocarboxylic dye at −3.31 eV (with 27% of electron density on the dye), (c) the LUMO+84 of the T2-catechol dye at −1.85 eV (with 31% of electron density on the dye), and (d) the LUMO+52 of T2-phosphonic dye at −2.41 eV (with 44% of electron density on the dye).

zero, the LUMO energy in the adsorbed oligothiophene dyes is weakly dependent on the chain size conversely to the situation reigning for the free dyes; this so-called "pinning effect" has been the subject of several theoretical studies [46,47,72]. At the opposite, when S is around 1, the oligothiophene chain length affects the LUMO energies in the adsorbed systems in a similar way as for the free molecules.

As illustrated in Table II, the calculated values of S are 0.42, 0.68, 0.89, and 0.93 for thiocarboxylic, carboxylic, phosphonic, and catechol dyes, respectively. Thus, the adsorption of thiocarboxylic and carboxylic dyes on the titania surface triggers a pronounced pinning effect for the LUMO of the dye, i.e., the LUMO energy level in the adsorbed dyes is slightly sensitive to the conjugation length conversely to the situation reigning for the free dyes.

This effect can be ascribed to the stronger electronic coupling between the LUMO of the carboxylic and thiocarboxylic dyes and the titania conduction band evidenced above. This is consistent with our previous study highlighting that no pinning is found when we decouple the conjugated chain from the titania cluster by inserting either a phenylene (PTn-Ph) or vinylene phenylene (PTn-Vi-Ph) moiety in a meta configuration [46]. From these results, it may be inferred that the pinning effect is triggered by a high electronic density on the anchoring group in the adsorbed dye. The actual LUMO weight on the anchoring group assigned as $W_{\text{ads}}^{\text{anc}}$ can be

TABLE II. LUMO energy (free dye, eV), LUMO energy (adsorbed dye, eV), energy shift (ΔE, eV), lifetime broadening ($\hbar\Gamma$, meV), computed injection time into the titania conduction band (τ, fs), LUMO weight on the anchoring group for the adsorbed dyes ($W_{\text{ads}}^{\text{anc}}$, %), and S ratio for Tn dyes.

Dyes		E_{LUMO} (free)	E_{LUMO} (adsorbed)	ΔE	$\hbar\Gamma$	τ	$W_{\text{ads}}^{\text{anc}}$	S
	T1	−2.13	−2.72	0.59	220	3.0	32	
	T2	−2.57	−3.04	0.47	125	5.3	27	
Carboxylic acid	T3	−2.77	−3.12	0.35	96	6.8	25	0.68
	T4	−2.89	−3.23	0.34	40	16.4	18	
	T5	−2.93	−3.27	0.34	35	18.9	15	
	T1	−2.50	−3.09	0.59	141	4.7	54	
	T2	−2.81	−3.21	0.40	81	8.1	42	
Thiocarboxylic acid	T3	−2.95	−3.34	0.39	44	15.0	33	0.42
	T4	−2.98	−3.27	0.29	68	9.7	33	
	T5	−3.00	−3.29	0.29	59	11.2	32	
	T1	−1.80	−2.06	0.26	60	10.9	20	
	T2	−2.27	−2.41	0.14	47	14.0	15	
Phosphonic acid	T3	−2.61	−2.71	0.10	28	23.4	10	0.89
	T4	−2.72	−2.75	0.03	20	32.2	8	
	T5	−2.83	−3.01	0.18	14	48.3	6	
	T1	−1.11	−1.22	0.11	25	26.8	16	
	T2	−1.71	−1.86	0.15	30	22.0	13	
Catechol	T3	−2.05	−2.18	0.13	38	17.1	8	0.93
	T4	−2.27	−2.29	0.02	29	22.6	8	
	T5	−2.45	−2.47	0.02	39	17.0	7	

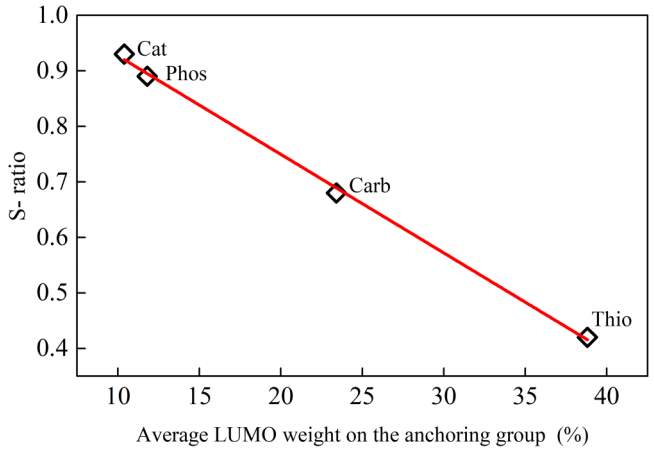

FIG. 7. S ratio vs the average LUMO weight on the anchoring group for Tn dyes.

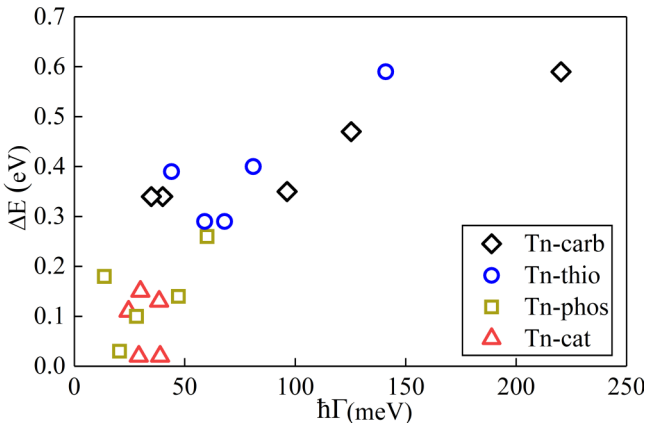

FIG. 8. LUMO energy shift vs lifetime broadening for Tn dyes.

estimated as follows:

$$W_{\text{ads}}^{\text{anc}} = \sum_i p_i^{\text{anc}} \quad p_i^{\text{anc}} = \sum_j^{A \in \text{anc}} \left(c_{ij}^A\right)^2 \Big/ \sum_j^n \left(c_{ij}^A\right)^2, \qquad (10)$$

where p_i^{anc} is the fraction of the molecular orbital i located on the anchoring group; the index i runs over all electronic levels in the energy interval making the total PDOS contribution on the molecule equal to 1.

If $W_{\text{ads}}^{\text{anc}}$ is small, the anchoring group bears only a small proportion of the LUMO electronic density. The results displayed in Table II do show that carboxylic acid and thiocarboxylic acid-based dyes have a higher LUMO weight on the anchoring group with respect to phosphonic and catechol dyes. This different behavior is mainly attributed to the fact that the carboxylic and thiocarboxylic acid groups have a good electron withdrawing ability while catechol has an electron donating ability. Particularly, the small LUMO weight on phosphonic acid is explained by the loss of π conjugation since the sp^2-hybridized dye LUMO weakly mixes with the sp^3-hybridized phosphonate group compared to the sp^2-hybridized carboxylic or thiocarboxylic group. Figure 7 clearly evidences that increasing the average LUMO weight on the anchoring group results in a decrease in the S ratio and hence an increase in the pinning effect strength. A substantial implication of the pinning effect is that the optical response of the oligothiophene dyes can be radically different when going from solution to the adsorbed system, *vide infra.*

C. Electron injection time

The electronic coupling strength between the dye LUMO and the titania conduction band is not only manifested by the LUMO energy shift and the pinning effect but also by the LUMO lifetime broadening. Interestingly, the level of broadening allows a direct estimation of the electron injection time by using the relation given in Eq. (8). The calculated lifetime broadenings and injection times for the oligothiophene dyes are listed in Table II. As expected from the previous considerations, a large lifetime broadening is computed for carboxylic dyes (35–220 meV) and thiocarboxylic dyes (59–141 meV), evidencing the strong dye-titania coupling already witnessed by the large shift of the LUMO level upon adsorption on titania. In contrast, a small lifetime broadening is computed for catechol dyes (25–39 meV) and phosphonic dyes (14–60 meV) as a result of the weak mixing between the dye LUMO and titania conduction-band states, leading in turn to longer injection times. Figure 8 nicely illustrates the correlation between the amplitude of the energy shift of the LUMO upon adsorption and the extent of its lifetime broadening with the conduction-band states of titania.

D. Optical properties

This section aims at elucidating the influence of the nature of the anchoring group on the optical response of oligothiophene dyes upon adsorption on TiO_2 cluster. For the sake of illustration, the absorption spectra of the free and adsorbed T2 and T5 simulated at TDDFT level are shown in Fig. 9; note that the Gaussian broadening used to generate the absorption spectra is set to $\sigma = 0.3$ eV and that the absorption spectra of the free and adsorbed dyes have been renormalized to have the same maximum intensity.

The spectra simulated for the adsorbed dyes displayed in Fig. 9 show that increasing the number of thiophene rings from 2 to 5 leads to a redshift of the lowest absorption band as predicted from the extension of the π-conjugation segment. The lowest intramolecular dye excited state transition energy as well as the calculated HOMO-LUMO gap are displayed in Table III. The redshift of the absorption spectra upon extending the chain length is fully in line with the decrease in the corresponding HOMO-LUMO gap (HL_{gap}).

More importantly, Fig. 9 indicates that the adsorption process gives rise to a systematic redshift of the absorption spectra. This redshift has been evaluated by computing the difference between the lowest excitation energy of the free dyes and the lowest intramolecular transition energy of the adsorbed dyes. In Fig. 9, T2-carboxylic, T5-carboxylic, T2-thiocarboxylic, and T5-thiocarboxylic exhibit a redshift of 0.5, 0.25, 0.57, and 0.24 eV, respectively. Conversely, a smaller shift is noticed for T2-phosphonic and T5-phosphonic (0.11 and 0.10 eV, respectively) while no shift is found for the T2-catechol and T5-catechol dyes.

This redshift results from an asymmetrical stabilization of the HOMO and LUMO levels upon adsorption on titania

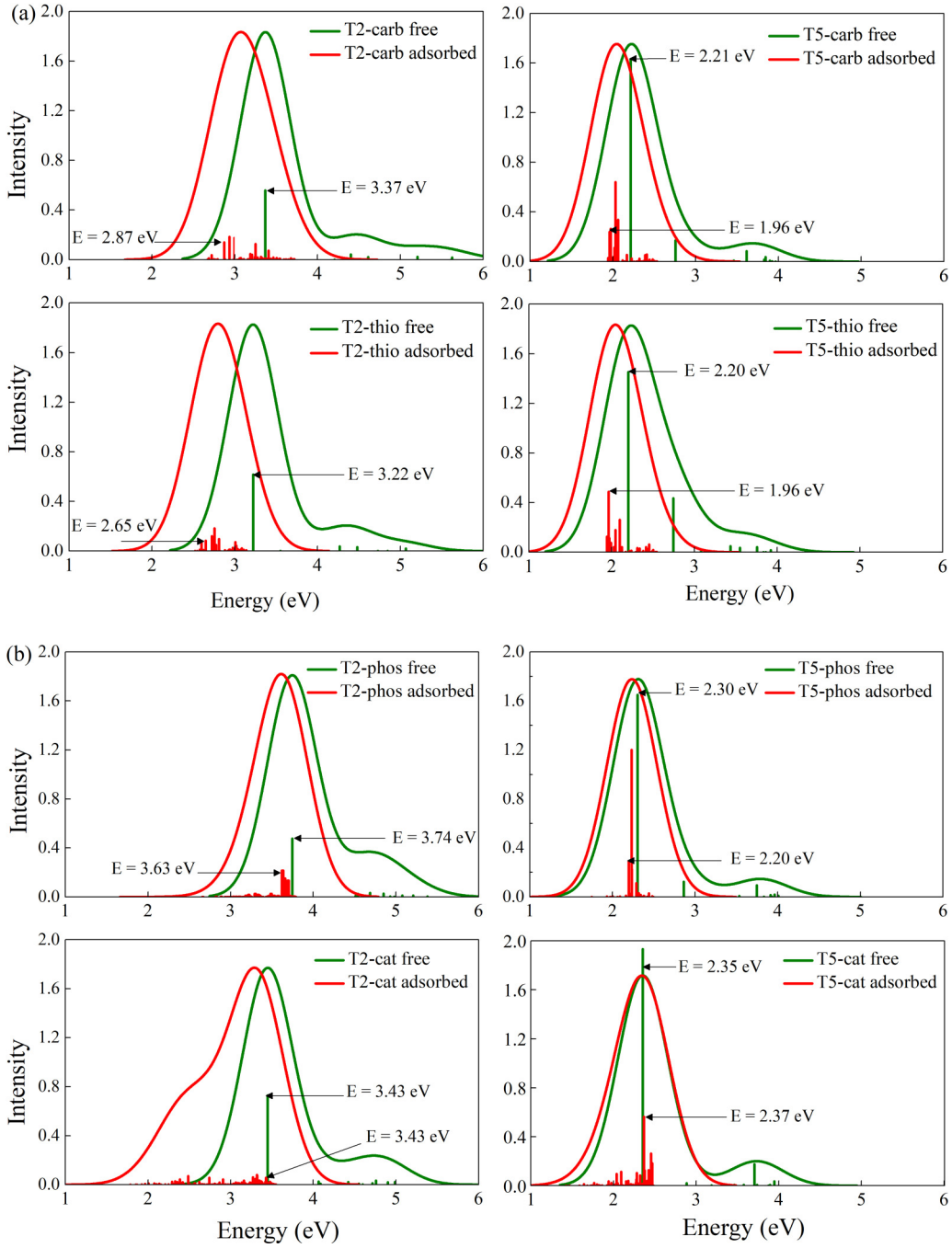

FIG. 9. Simulated UV-Vis absorption spectra of free (a) T2-carboxylic, T5-carboxylic, T2-thiocarboxylic, T5-thiocarboxylic, (b) T2-phosphonic, T5-phosphonic, T2-catechol, and T5-catechol versus adsorbed on the TiO_2 cluster. The lowest intramolecular transition energy is also pointed with an arrow.

cluster. As reported in the previous section, this stabilization is more pronounced for the LUMO level, which leads to a decrease in the HL_{gap} of the adsorbed dyes with respect to that of the corresponding free dyes (see Table III). Since the stabilization of the LUMO levels are stronger for carboxylic and thiocarboxylic dyes than for the phosphonic and catechol dyes, the induced redshift is thus larger for the former systems. Remarkably, when increasing the number of thiophene rings from 2 to 5, the redshift of the lowest absorption band for the adsorbed carboxylic and thiocarboxylic dyes is smaller than that for the corresponding free systems; in the case of the carboxylic (thiocarboxylic) acid, the redshift amounts to 1.16 eV (1.02 eV) for the free dyes while 0.91 eV (0.69 eV) is computed for the adsorbed systems. In contrast, the redshift upon increasing the chain size is similar for both free and adsorbed phosphonic and catechol dyes (i.e., 1.06 eV for catechol and 1.44 eV for phosphonic acid), as a result of the weaker degree of pinning effect.

Noteworthy, the behavior of the adsorbed T2-catechol is quite different compared to the other adsorbed dyes since a new low-energy shoulder appears upon adsorption around 2.48 eV (500 nm). The analysis of the TD-DFT results (see

TABLE III. HOMO-LUMO differences (HL_{gap}, eV) and lowest intramolecular transition energy for free and adsorbed Tn dyes.

	HL_{gap}		Lowest transition energy	
Dyes	free	adsorbed	free	adsorbed
T2-carb	3.53	3.34	3.37	2.87
T3-carb	2.89	2.88	2.77	2.53
T4-carb	2.53	2.46	2.39	2.19
T5-carb	2.39	2.25	2.21	1.96
T2-thio	3.41	3.08	3.22	2.65
T3-thio	2.83	2.60	2.67	2.29
T4-thio	2.56	2.46	2.38	2.11
T5-thio	2.41	2.27	2.20	1.96
T2-phos	4.07	4.02	3.74	3.63
T3-phos	3.22	3.23	2.99	2.93
T4-phos	2.80	2.95	2.59	2.63
T5-phos	2.50	2.46	2.30	2.20
T2-cat	3.75	3.75	3.43	3.43
T3-cat	3.23	3.21	2.97	2.90
T4-cat	2.84	3.06	2.60	2.69
T5-cat	2.59	2.71	2.35	2.37

Table SV of the Supplemental Material [63]) reveals that the main contributions to this shoulder are excitations from the HOMO orbital strongly localized on the dye to LUMO+26, LUMO+27 and LUMO+30 orbitals predominantly localized on the cluster. These optical transitions thus correspond to a direct injection mechanism described as a direct photoexcitation from the HOMO of the dye to the titania conduction band without any implication of the intramolecular dye excited state [28,31,47]. To further shed light on this shoulder, the partial density of states (PDOS) of the T2-catechol dye has been computed and displayed in Fig. 10(a). The first level with a high contribution of the T2-catechol molecule (that corresponds to the dye LUMO) is located well into the conduction band (∼1.7 eV above the conduction-band edge) while the frontier virtual states are mostly located on the titania cluster without any noticeable contribution from the dye molecule. These mixed states [see Fig. 10(a)] coincide with the overall maximum PDOS of TiO_2 in this energy range and the interaction between the dye unoccupied levels and the conduction band of titania is significant. An excitation from the HOMO of the dye to these levels is responsible for the direct electron injection and for the new shoulder in the spectrum of TiO_2 upon adsorption of T2-catechol.

Nevertheless, the photoinduced electron transfer for the carboxylic dyes, thiocarboxylic dyes, phosphonic dyes, and catechol dyes with chains longer than T2 occurs essentially via an indirect injection mechanism (type I) since the excitations in the lowest absorption band show a significant dye-centered character (see Sec. II of the Supplemental Material [63] for details) without the apparition of any new low-energy band. In this case, the broadened dye LUMO yields the first peak above the conduction-band edge and no mixed states are formed in contrast to the situation prevailing in T2-catechol dye [see Fig. 10(b) for T2-thiocarboxylic]. This implies that the electron is initially excited from the HOMO to the LUMO level before getting injected in the

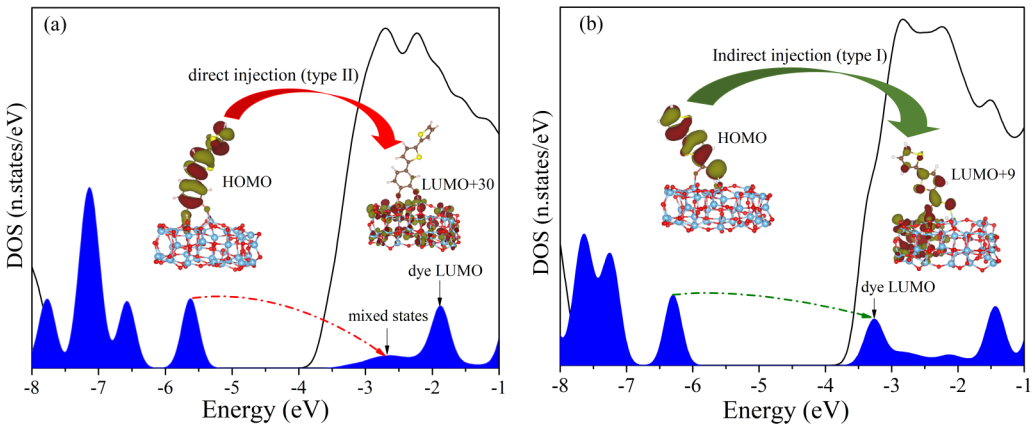

FIG. 10. (a) T2-catechol dye PDOS (blue line), TiO_2 PDOS (black line), HOMO and LUMO+30 of the adsorbed T2-catechol on the TiO_2 cluster. (b) T2-thiocarboxylic dye PDOS (blue line), TiO_2 PDOS (black line), HOMO and LUMO+9 of the adsorbed T2-thiocarboxylic on the TiO_2 cluster. The PDOS have been broadened with a Gaussian function with a width $\sigma = 0.3$ eV and the dye LUMO value calculated from the Newns-Anderson approach is indicated by the arrow.

titania conduction band with injection times similar to those calculated in the former section. It is worth emphasizing that the back-electron transfer (recombination parasitic processes) is highly promoted in the type-II injection compared to type I, which may decrease the efficiency of shorter-chain catechol dyes. Therefore, the nature of the anchoring group not only reflects on the absorption spectra of the adsorbed dyes, but also on the overall efficiency of DSSCs by dictating the operative injection mechanism.

V. CONCLUSION

The modifications in the electronic and optical properties of a series of oligothiophene dyes upon adsorption on a titania anatase (101) surface with different anchoring groups have been theoretically studied using density functional theory (DFT) and time-dependent DFT.

The interaction at the dye-semiconductor interface has been explored by using the Newns-Anderson approach. The LUMO levels of oligothiophene dyes adsorbed via carboxylic and thiocarboxylic acids are highly shifted upon adsorption as a result of the strong hybridization at the interface giving rise to a pronounced pinning effect while a slight shift and a weak pinning effect are observed for oligothiophene dyes adsorbed via phosphonic acid and catechol. This different behavior is mainly attributed to the higher electronic density on the anchoring group for carboxylic and thiocarboxylic acid compared to catechol and phosphonic acid. Besides, we have estimated the electron injection time from the dye to the TiO_2 semiconductor through the lifetime broadening of the dye LUMO triggered by the interaction with the conduction-band states of the semiconductor. Our results indicate that carboxylic and thiocarboxylic oligothiophene dyes display a larger lifetime broadening and hence faster electron injection times. In contrast, the oligothiophene dyes adsorbed on titania via phosphonic acid and catechol yield smaller broadenings and thus slower injection times. This discrepancy is substantially ascribed to the donor character of the catechol, that polarizes the LUMO away from the dye-titania interface and the loss of π conjugation in phosphonic acid since the sp^2-hybridized dye LUMO weakly mixes with the sp^3-hybridized phosphonate group compared to the sp^2-hybridized carboxylic or thiocarboxylic group, which significantly reduce the electronic coupling between the dye and titania surface.

The simulated absorption spectra of the free and adsorbed dyes obtained with TD-DFT calculations have shown that the carboxylic and thiocarboxylic oligothiophene dyes display a large redshift upon adsorption owing to the pronounced LUMO stabilization whereas a slight redshift is noticed for phosphonic and catechol oligothiophene dyes. Due to the strong pinning effect, the redshift of the lowest absorption band with increasing chain size is less sensitive to the conjugation length for the adsorbed carboxylic and thiocarboxylic dyes when compared to the situation reigning for the corresponding free dyes. In contrast, the same evolution with chain size are obtained for free and adsorbed phosphonic and catechol dyes. This pinning effect could be experimentally revealed by considering a series of dyes varying by their chain length or via the introduction of electroactive substituents. We hope this work will inspire further experimental studies in this direction.

Altogether, this study has highlighted the critical role of the choice of the anchoring group in DSSCs and that strategies to minimize the electron injection times considering dyes in solution may prove to be inadequate since adsorption of the dyes onto the semiconductor surface can induce a significant perturbation of the electronic and optical properties of the dyes. In other words, the choice of a suitable anchoring group is not unique and depends whether the prime requirement is to (i) maintain the electronic and optical properties of the isolated dyes upon adsorption through the use of anchoring groups promoting a weak interfacial electronic coupling (such as catechol and phosphonic acid), though at the expense of longer electron injection times, or (ii) to achieve fast electron injection times by using anchoring groups promoting a strong interfacial coupling (such as carboxylic acid and thiocarboxylic acid) albeit with the risk of a significant perturbation of the electronic and optical properties of the dyes upon adsorption.

ACKNOWLEDGMENTS

This work has been supported by Centre National pour la Recherche Scientifique et Technique (CNRST) au Maroc and by the Belgian National Fund for Scientific Research (FNRS). Computational resources were provided by the Consortium des Equipements de Calcul Intensif (CECI) funded by F.R.S.-FNRS under Grant No. 2.5020.11. J.C. is an FNRS research director.

[1] B. O'regan and M. Grätzel, Nature (London) **353**, 737 (1991).

[2] Z. Ning, Y. Fu, and H. Tian, Energy Environ. Sci. **3**, 1170 (2010).

[3] M. Pastore, T. Etienne, and F. De Angelis, J. Mater. Chem. C **4**, 4346 (2016).

[4] Y. Cao, Y. Bai, Q. Yu, Y. Cheng, S. Liu, D. Shi, F. Gao, and P. Wang, J. Phys. Chem. C **113**, 6290 (2009).

[5] M. A. Green, E. D. Dunlop, J. Hohl-Ebinger, M. Yoshita, N. Kopidakis, and X. Hao, Prog. Photovoltaics Res. Appl. **28**, 629 (2020).

[6] D. Kuang, C. Klein, S. Ito, J.-E. Moser, R. Humphry-Baker, N. Evans, F. Duriaux, C. Grätzel, and S. M. Zakeeruddin, Adv. Mater. **19**, 1133 (2007).

[7] D. Kuang, S. Ito, B. Wenger, C. Klein, J.-E. Moser, R. Humphry-Baker, S. M. Zakeeruddin, and M. Grätzel, J. Am. Chem. Soc. **128**, 4146 (2006).

[8] S. A. Haque, E. Palomares, B. M. Cho, A. N. Green, N. Hirata, D. R. Klug, and J. R. Durrant, J. Am. Chem. Soc. **127**, 3456 (2005).

[9] S. A. Haque, S. Handa, K. Peter, E. Palomares, M. Thelakkat, and J. R. Durrant, Angew. Chem. Int. Ed. **44**, 5740 (2005).

[10] D. Kuang, C. Klein, S. Ito, J. E. Moser, R. Humphry-Baker, S. M. Zakeeruddin, and M. Graetzel, Adv. Funct. Mater. **17**, 154 (2007).

[11] M. R. Elmorsy, R. Su, A. A. Fadda, H. Etman, E. H. Tawfik, and A. El-Shafei, Dyes Pigm. **156**, 348 (2018).

[12] M. K. Nazeeruddin, A. Kay, I. Rodicio, R. Humphry-Baker, E. Müller, P. Liska, N. Vlachopoulos, and M. Grätzel, J. Am. Chem. Soc. **115**, 6382 (1993).

[13] N. I. Beedri, P. K. Baviskar, V. P. Bhalekar, C. V. Jagtap, A. M. Asiri, S. R. Jadkar, and H. M. Pathan, Phys. Status Solidi A **215**, 1800236 (2018).

[14] K. Xu and L. Zhang, Dyes Pigm. **173**, 107925 (2020).

[15] M. K. Nazeeruddin, P. Pechy, and M. Grätzel, Chem. Commun. 1705 (1997), doi: 10.1039/A703277C.

[16] R. Boaretto, S. Carli, S. Caramori, C. Bignozzi, D. Saccone, C. Magistris, C. Barolo, and G. Viscardi, Dalton Trans. **46**, 16390 (2017).

[17] S. Shalini, R. Balasundaraprabhu, T. S. Kumar, N. Prabavathy, S. Senthilarasu, and S. Prasanna, Int. J. Energy Res. **40**, 1303 (2016).

[18] K. Hara, Z.-S. Wang, T. Sato, A. Furube, R. Katoh, H. Sugihara, Y. Dan-oh, C. Kasada, A. Shinpo, and S. Suga, J. Phys. Chem. B **109**, 15476 (2005).

[19] Z.-S. Wang, Y. Cui, Y. Dan-oh, C. Kasada, A. Shinpo, and K. Hara, J. Phys. Chem. C **112**, 17011 (2008).

[20] T. Horiuchi, H. Miura, and S. Uchida, Chem. Commun., 3036 (2003), doi: 10.1039/B307819A.

[21] H. Tanaka, A. Takeichi, K. Higuchi, T. Motohiro, M. Takata, N. Hirota, J. Nakajima, and T. Toyoda, Sol. Energy Mater. Sol. Cells **93**, 1143 (2009).

[22] R. Chen, X. Yang, H. Tian, and L. Sun, J. Photochem. Photobiol. A **189**, 295 (2007).

[23] Y. Hao, X. Yang, J. Cong, H. Tian, A. Hagfeldt, and L. Sun, Chem. Commun., 4031 (2009), doi: 10.1039/B908396K.

[24] C. Li *et al.*, ChemSusChem **1**, 615 (2008).

[25] Y. Jin, J. Hua, W. Wu, X. Ma, and F. Meng, Synth. Met. **158**, 64 (2008).

[26] K. Tanaka, K. Takimiya, T. Otsubo, K. Kawabuchi, S. Kajihara, and Y. Harima, Chem. Lett. **35**, 592 (2006).

[27] S. Tan, J. Zhai, H. Fang, T. Jiu, J. Ge, Y. Li, L. Jiang, and D. Zhu, Chem. - Eur. J. **11**, 6272 (2005).

[28] R. Sánchez-de-Armas, J. Oviedo, M. Á. San Miguel, and J. F. Sanz, J. Phys. Chem. C **115**, 11293 (2011).

[29] J. Li, I. Kondov, H. Wang, and M. Thoss, J. Phys. Chem. C **114**, 18481 (2010).

[30] Y. Wang, K. Hang, N. A. Anderson, and T. Lian, J. Phys. Chem. B **107**, 9434 (2003).

[31] P. Persson, R. Bergström, and S. Lunell, J. Phys. Chem. B **104**, 10348 (2000).

[32] R. Sánchez-de-Armas, M. San-Miguel, J. Oviedo, and J. F. Sanz, Comput. Theor. Chem. **975**, 99 (2011).

[33] R. L. Blackbourn, C. S. Johnson, and J. T. Hupp, J. Am. Chem. Soc. **113**, 1060 (1991).

[34] H. N. Ghosh, J. B. Asbury, Y. Weng, and T. Lian, J. Phys. Chem. B **102**, 10208 (1998).

[35] K. A. Walters, D. A. Gaal, and J. T. Hupp, J. Phys. Chem. B **106**, 5139 (2002).

[36] M. Khoudiakov, A. R. Parise, and B. S. Brunschwig, J. Am. Chem. Soc. **125**, 4637 (2003).

[37] B.-K. An, W. Hu, P. L. Burn, and P. Meredith, J. Phys. Chem. C **114**, 17964 (2010).

[38] J. Schnadt and J. N. O'Shea, J. Chem. Phys. **119**, 12462 (2003).

[39] R. R. Frontiera, J. Dasgupta, and R. A. Mathies, J. Am. Chem. Soc. **131**, 15630 (2009).

[40] J. M. Rehm, G. L. McLendon, Y. Nagasawa, K. Yoshihara, J. Moser, and M. Grätzel, J. Phys. Chem. **100**, 9577 (1996).

[41] L. Gundlach, R. Ernstorfer, and F. Willig, J. Phys. Chem. C **111**, 13586 (2007).

[42] L. Gundlach, T. Letzig, and F. Willig, J. Chem. Sci. **121**, 561 (2009).

[43] A. Hagfeldt, G. Boschloo, L. Sun, L. Kloo, and H. Pettersson, Chem. Rev. **110**, 6595 (2010).

[44] F. Ambrosio, N. Martsinovich, and A. Troisi, J. Phys. Chem. letters **3**, 1531 (2012).

[45] L. Zhang and J. M. Cole, ACS Appl. Mater. Interfaces **7**, 3427 (2015).

[46] L. Lasser, E. Ronca, M. Pastore, F. De Angelis, J. Cornil, R. Lazzaroni, and D. Beljonne, J. Phys. Chem. C **119**, 9899 (2015).

[47] I. Arbouch, D. Cornil, Y. Karzazi, B. Hammouti, R. Lazzaroni, and J. Cornil, Phys. Chem. Chem. Phys. **19**, 29389 (2017).

[48] D. Beljonne and J. Cornil, *Multiscale Modelling of Organic and Hybrid Photovoltaics* (Springer, Berlin Heidelberg, 2014).

[49] N. Martsinovich and A. Troisi, Energy Environ. Sci. **4**, 4473 (2011).

[50] M. J. Lundqvist, M. Nilsing, P. Persson, and S. Lunell, Int. J. Quantum Chem. **106**, 3214 (2006).

[51] R. W. G. Wyckoff, *Crystal Structures*, 2nd ed. (Interscience, New York, 1963).

[52] P. Persson, J. C. M. Gebhardt, and S. Lunell, J. Phys. Chem. B **107**, 3336 (2003).

[53] F. De Angelis, A. Tilocca, and A. Selloni, J. Am. Chem. Soc. **126**, 15024 (2004).

[54] F. De Angelis, S. Fantacci, A. Selloni, M. K. Nazeeruddin, and M. Grätzel, J. Phys. Chem. C **114**, 6054 (2010).

[55] A. Vittadini, A. Selloni, F. P. Rotzinger, and M. Grätzel, Phys. Rev. Lett. **81**, 2954 (1998).

[56] L.-M. Liu, S.-C. Li, H. Cheng, U. Diebold, and A. Selloni, J. Am. Chem. Soc. **133**, 7816 (2011).

[57] A. Vittadini, A. Selloni, F. Rotzinger, and M. Grätzel, J. Phys. Chem. B **104**, 1300 (2000).

[58] C. Pérez León, L. Kador, B. Peng, and M. Thelakkat, J. Phys. Chem. B **110**, 8723 (2006).

[59] R. Luschtinetz, J. Frenzel, T. Milek, and G. Seifert, J. Phys. Chem. C **113**, 5730 (2009).

[60] R. Luschtinetz, S. Gemming, and G. Seifert, Eur. Phys. J. Plus **126**, 98 (2011).

[61] A. O. T. Patrocínio, E. B. Paniago, R. M. Paniago, and N. Y. M. Iha, Appl. Surf. Sci. **254**, 1874 (2008).

[62] K. L. Syres, A. G. Thomas, W. R. Flavell, B. F. Spencer, F. Bondino, M. Malvestuto, A. Preobrajenski, and M. Grätzel, J. Phys. Chem. C **116**, 23515 (2012).

[63] See Supplemental Material at http://link.aps.org/supplemental/10.1103/PhysRevMaterials.4.115401 for more details about the binding energy and the electron injection mechanisms.

[64] J. P. Perdew, K. Burke, and M. Ernzerhof, Phys. Rev. Lett. **77**, 3865 (1996).

[65] G. te Velde, F. M. Bickelhaupt, E. J. Baerends, C. Fonseca Guerra, S. J. van Gisbergen, J. G. Snijders, and T. Ziegler, J. Comput. Chem. **22**, 931 (2001).

[66] M. J. Frisch *et al.*, *Gaussian 09 Revisions* (Gaussian Inc., Wallingford CT, 2016), https://gaussian.com/g09citation/.

[67] J. P. Muscat and D. M. Newns, Prog. Surf. Sci. **9**, 1 (1978).

[68] P. Persson, M. J. Lundqvist, R. Ernstorfer, W. Goddard, and F. Willig, J. Chem. Theory Comput. **2**, 441 (2006).

[69] P. Péchy, F. P. Rotzinger, M. K. Nazeeruddin, O. Kohle, S. M. Zakeeruddin, R. Humphry-Baker, and M. Grätzel, J. Chem. Soc. Chem. Commun., 65 (1995), doi: 10.1039/C39950000065.

[70] M. Nilsing, S. Lunell, P. Persson, and L. Ojamäe, Surf. Sci. **582**, 49 (2005).

[71] R. Sánchez-de-Armas, M. San-Miguel, J. Oviedo, A. Marquez, and J. Sanz, Phys. Chem. Chem. Phys. **13**, 1506 (2011).

[72] V. Diez-Cabanes, S. R. Gonzalez, S. Osella, D. Cornil, C. Van Dyck, and J. Cornil, Adv. Theory Simul. **1**, 1700020 (2018).